Nanoscale

Accepted Manuscript

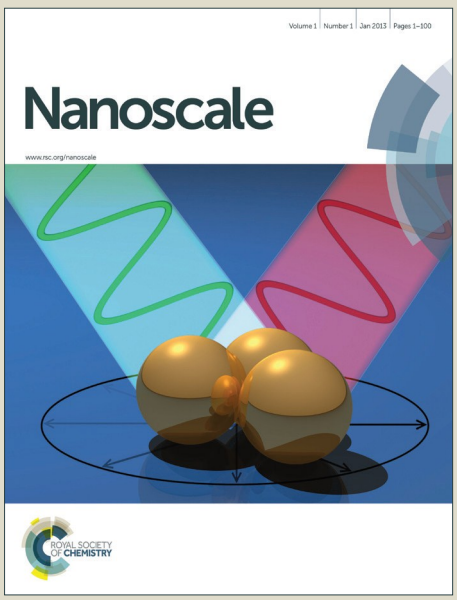

ROYAL SOCIETY OF CHEMISTRY

www.rsc.org/nanoscale

Nanoscale

Paper

Enhanced Photovoltaic Performance of Ultrathin Si Solar Cells via Semiconductor Nanocrystal Sensitization: Energy Transfer vs. Optical Coupling Effects†

Received 00th January 20xx,
Accepted 00th January 20xx

DOI: 10.1039/x0xx00000x

www.rsc.org/

Son Hoang,[a] Ahsan Ashraf,[b,c] Matthew D. Eisaman,[b,c,d] Dmytro Nykypanchuk,[*,a] and Chang-Yong Nam,[*,a]

Excitonic energy transfer (ET) offers exciting opportunities for advances in optoelectronic devices such as solar cells. While recent experimental attempts have demonstrated its potential in both organic and inorganic photovolatics (PVs), what remains to be addressed is quantitative understading of how different ET modes contubute to PV performance and how ET contribution is differentiated from classical optical coupling (OC) effects. In this study, we implenent ET scheme using a PV device platform, comprising CdSe/ZnS nanocrystal energy donor and 500 nm-thick ultrathin Si acceptor layers, and present quantiative mechanistic description on how different ET modes, distinguished from OC effects, increase light absorption and PV effeiciency. We find nanoscrystal sensitization enhances the short circuit current of ultrathin Si solar cells by up to 35%, of which the efficient ET, primarily driven by long-range radiative mode, contributes to 38% of the total current enhacement. These results not only confirm the positive impact of ET but also provide a guideline for rationally combining ET and OC effects for improved light harvesting in PV and other optoelectronic devices.

1 Introduction

Light harvesting via excitonic energy transfer (ET), as exemplified in the natural photosynthesis,[1-3] has inspired significant research efforts for understanding and designing ET-based light harvesting systems for solar energy conversion and other optoelectronic applications.[4-9] For molecular systems, the ET mechanism is relatively well understood,[1,10,11] and recently a few groups demonstrated applications of ET in dye-sensitized solar cells (DSSCs)[6,7,12] and organic photovoltaic (PV) devices composed of either bulk heterojunction (BHJ)[13] or multi-stacked active layers.[14] In these devices, the Förster-type non-radiative ET (NRET) was the dominant ET mechanism which is effective for the energy donor-acceptor separation of a few nanometers due to its fast decaying ET rate with increasing distance. The sensitization of solar cells employing NRET is thus expected to limit the effective thickness of the energy harvesting donor layer to a few nanometers as the energy donor added beyond would rather block incident photons, hampering the overall PV power conversion efficiency (PCE). On the other hand, the radiative ET (RET), occurring via the transfer of excitation energy by radiative decay of a donor and subsequent reabsorption of the emitted radiation by an acceptor, can remain efficient for the separation as far as a few tens of nanometers,[4,15] potentially allowing a thicker energy donor layer of more effective light-harvesting ability and hence enhanced contribution of overall ET to the PCE of solar cells.

Meanwhile, for the implementation of ET in inorganic PVs, a new device architecture that combines energy donor layers capable of strong light absorption with energy acceptors made of high-carrier-mobility materials has been suggested.[4,16,17] Particularly, the use of semiconductor nanocrystal (NC) layers as energy donors in conjunction with a crystalline thin-film Si energy acceptor has been highlighted in a series of optical studies,[15,18,19] where the excitonic sensitization of Si via NC energy donors is predicted to take full advantage of the large absorption cross-section and tunable optical properties of NCs, in tandem with the low exciton binding energy and high carrier mobility of Si.[4,15] Recently, it was shown that such a NC sensitization could indeed improve the performance of ultrathin Si-based photodetectors[20] as well as thick Si nanowire solar cells,[21] where optical spectroscopy was used to confirm the presence of ET process. However, important fundamental questions remain regarding quantitative contribution of different ET modes to the experimentally measured PV energy conversion performance and how such ET contributions can be differentiated from more classical optical coupling effects.

In this work, we report the ET-driven enhancement of PV performance in an ultrathin Si solar cell architecture consisting of semiconductor NC energy donor layers atop an ultrathin Si energy

[a] Center for Functional Nanomaterials, Brookhaven National Laboratory, Upton, New York 11973, United States, E-mail: dnykypan@bnl.gov (D.N.), cynam@bnl.gov (C.-Y.N.).
[b] Sustainable Energy Technologies Department, Brookhaven National Laboratory, Upton, New York 11973, United States.
[c] Department of Physics and Astronomy, Stony Brook University, Stony Brook, New York 11794, United States.
[d] Department of Electrical and Computer Engineering, Stony Brook University, Stony Brook, New York 11794, United States

†Electronic Supplementary Information (ESI) available: Details of theoretical calculation of ET efficiency, inter-NC energy transfer efficiency, histograms of PV characteristics, and simulated absorption of NC layer and Si. See DOI: 10.1039/x0xx00000x

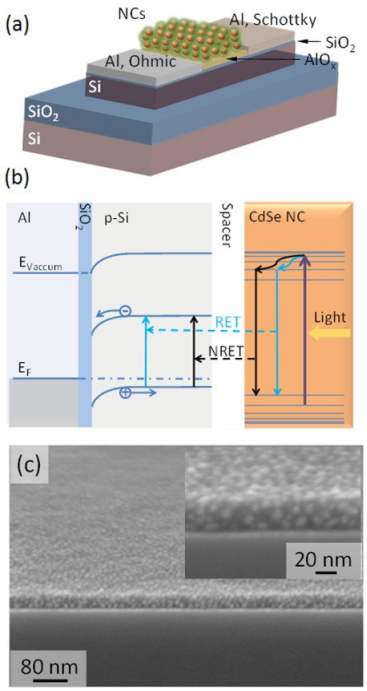

Fig. 1 (a) Schematic structure of ET-based hybrid solar cell consisting of semiconductor NCs and ultrathin Si as energy donor and acceptor, respectively. (b) Energy diagram illustrating ET-induced light absorption in Si and subsequent charge separation and extraction by Schottky junction. (c) Scanning electron microscopy (SEM) micrographs of CdSe/ZnS NC energy donor layer deposited on the active channel of an ultrathin Si Schottky junction solar cell.

acceptor with an incorporated in-plane Schottky junction and controlled thickness of donor-acceptor spacer made of aluminium oxide (AlO_x). The well-defined layered device geometry not only decouples the NC energy donor layer from the charge transport and extraction processes in the Si solar cell but also enables us to combine complementary investigative methods, including PV device characterization, time-resolved optical spectroscopy, transfer-matrix optical simulation, and dipole radiation theory calculation. By using this approach, we establish a quantitative mechanistic understanding on how different ET modes, distinguished from the intrinsic optical interference effects, contribute to the light harvesting in functioning inorganic solar cells and clearly demonstrate the positive contribution of ET to the enhancement of the device PCE, primarily driven by the effective long-range RET that improves the solar spectrum absorption in the ultrathin Si active layer.

2 Results and Discussion

Design of Ultrathin Si Schottky Junction Solar Cells with NC Energy Donor Layers

The ultrathin Si Schottky-junction solar cell employing NC energy donor layers comprises a p-type Si on insulator (SOI) substrate (500 nm thick Si layer), incorporating in-plane Al ohmic/Schottky contacts, and an exposed Si channel active area (0.75 mm (width) × 10 μm (length), optimized for efficient charge collection and reliable device fabrication), which is coated with 3–4 monolayers of CdSe/ZnS core-shell NC energy donor (inner inorganic particle diameter: 4.5 nm; polymer ligand coating thickness: 3.5 nm)[15] with an AlO_x spacer of varying thickness between Si and NC layers (Fig. 1(a)). Here the incident photon energy absorbed by the NC layer is transferred to the Si channel, via either the oscillating electrostatic dipole field of excitons in NC (NRET) or the radiative decay (i.e., photoluminescence (PL)) of NC excitation (RET), to create electron-hole pairs in Si that are separated and extracted by the in-plane Schottky junction (Fig. 1(b)). The device architecture is designed to provide a platform for a systematic and quantitative analysis of influences of different ET modes on the PV device performance. The main related design feature is the in-plane Schottky junction geometry that exposes the active channel of pristine Si on top of the device surface. This allows: (a) Simple fabrication of robust model base solar cells; (b) precise control over the thicknesses of spacer (AlO_x) and CdSe/ZnS NC energy donor layers, which critically impact the mode and efficiency of ET and, consequently, the extent of any enhancement in PV performance; (c) well-defined layered device geometry suitable for cross-interrogation of ET effects by theoretical analysis and optical simulation. Meanwhile, the thickness of NC energy donor layer applied to the ultrathin Si solar cell is chosen to be 30–35 nm, equivalent to 3–4 monolayers (Fig. 1(c)), in order to balance an appreciable light absorption and efficient ET from NCs to Si. Excessively thick NC layers (e.g., >100 nm) would display a low ET efficiency despite a good optical absorption as the photon energy absorbed by top NC layers may not be efficiently transferred to the bottom Si. Despite the relatively small thickness of the NC energy donor layer that we apply, the device architecture consisting of multiple dielectric layers creates interference effects and, in fact, can result in an enhanced light absorption within the NC layer and, consequently, significant contribution to the ET-driven enhancement of the light harvesting in the solar cell as discussed in detail later.

Influence of NC on the Ultrathin Si Solar Cell PV Performance

We find that the application of NC layers on ultrathin Si indeed enhances the device PV performance of ultrathin Si solar cells. We first compare the PV performances of ultrathin Si solar cells with and without the applied CdSe/ZnS NC energy donor layer (four NC monolayers) for the case of minimum spacer thickness (1.7 nm thick SiO_2 without AlO_x), which is expected to achieve the highest ET efficiency from the NC energy donor layer. Fig. 2(a) displays a representative current density-voltage (*J-V*) characteristics of ultrathin Si Schottky junction solar cells under the air mass 1.5 global (AM1.5G) and 1 Sun (100 mW/cm^2) conditions, before and after the deposition of four monolayers of CdSe/ZnS NCs (~35 nm thick). The most remarkable change the NC layer imparts to the PV performance is the enhancement of short circuit current density (J_{SC}) by ~35% to 8.7 ± 1.6 mA/cm^2 from 6.4 ± 1.3 mA/cm^2 of the control device, which primarily drives the improvement in the corresponding PCE by ~45% from 1.08 ± 0.19% to 1.60 ± 0.21%. On the other hand, with the addition of NC layer, the open circuit voltage (V_{OC}) and fill factor (*FF*) remain largely unchanged at 0.34 ±

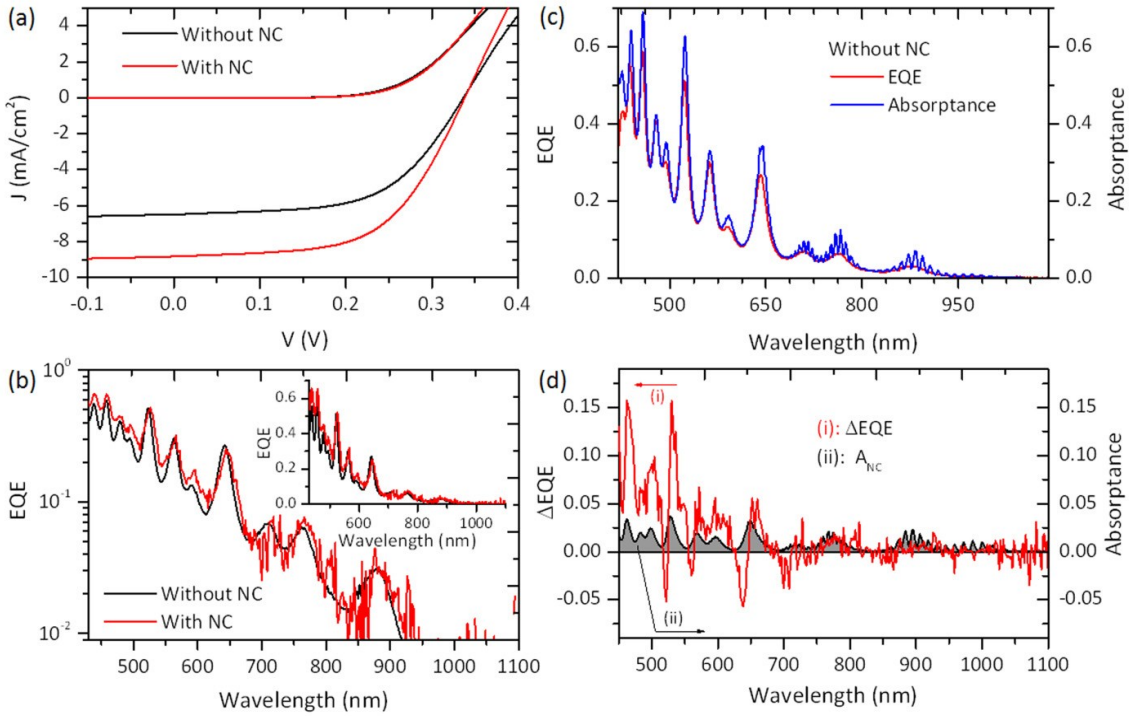

Fig. 2 (a) Representative PV *J-V* characteristics of ultrathin Si Schottky junction solar cells before (black) and after (red) the application of the CdSe/ZnS energy donor layer, measured under dark and 1 Sun AM1.5G illumination conditions. (b) Typical EQE spectra (semi-log scale) of the ultrathin Si solar cells before (black) and after (red) the deposition of the NC layer (inset: a linear scale EQE plot). (c) Composite plots of the EQE spectrum (red) of the solar cell without the NC layer and the simulated absorptance spectrum (blue) of the 500 nm thick ultrathin Si layer within the same device geometry. (d) Comparison of the gain in EQE (ΔEQE = EQE (with NC) – EQE (without NC), red) and the simulated absorptance spectrum of the CdSe/ZnS NC layer (A_{NC}, black) within the device structure.

0.05 V and 0.56 ± 0.06, respectively, similar to 0.32 ± 0.07 V and 0.55 ± 0.06 of the control ultrathin Si solar cell (all values presented here are the averages obtained from over 15 unique devices for each conditions. See Fig. S1†). This observation confirms that the NC layer does not participate or interfere with the charge transport processes occurring in the base ultrathin Si solar cells. We note that the use of in-plane Schottky junction (i.e., low V_{OC}) and the low optical absorptance of ultrathin Si result in the modest base device PCE but these design features enable a facile fabrication of reliable model devices where the influences of ET on the measured PV performance can be quantitatively delineated.

By investigating the device external quantum efficiency (EQE) and the optical absorptions of each component layers in the device structure, we identify that the observed enhancement in J_{SC} originates from two major factors, one caused by pure optical effects intrinsic to the device structure composed of multiple dielectric layers, and the other arising due to the genuine influences of ET from the NC energy donor layer. In conventional solar cells, dielectric coatings have been widely utilized as anti-reflective layers to improve the light harvesting by the active layer in solar cells.[22] A similar consideration may apply to the NC layer on the ultrathin Si, which potentially increases the amount of light absorbed in the ultrathin Si layer by enhancing the *optical coupling*. Once such an optical effect is quantified, the exclusive contribution of the ET from the NC layer can be isolated. To quantify the optical effect, we obtain the spectral absorptances exerted by the respective NC layer and ultrathin Si within the device architecture by combining the transfer-matrix optical simulation[23] and the experimental spectroscopic ellipsometry measurement of optical constants of each component layer (i.e., CdSe/ZnS NC layer, AlO_x spacer, SiO_2, and Si, Fig. S2 and S3†). The accuracy of this approach is verified by a standard test comparing simulated and experimentally measured angle-dependent reflectance of a control Si substrate. Aided by this analysis platform, we verify the exclusive contribution of ET to the improvement of light absorption in the ultrathin Si by understanding the change in measured EQE spectrum of ultrathin Si solar cells upon the application of the CdSe/ZnS NC layer.

The EQE spectra of both ultrathin Si solar cells with and without the NC layer feature multiple peaks, which originate from the intrinsic interference phenomenon in the SOI-substrate-based device structure having multiple dielectric layers (Fig. 2(b)). The simulated absorptance spectrum of the ultrathin Si layer within the solar cell without the NC layer (A_{Si}) exactly replicates the spectral shape of the EQE including the multiple peaks (Fig. 2(c)), confirming the anticipated optical interference effects and the accuracy of the simulation method. When analyzing the EQE spectra of ultrathin Si solar cells before and after the NC layer application (Fig. 2(b)), one apparent difference is the overall increased EQE with the NC layer

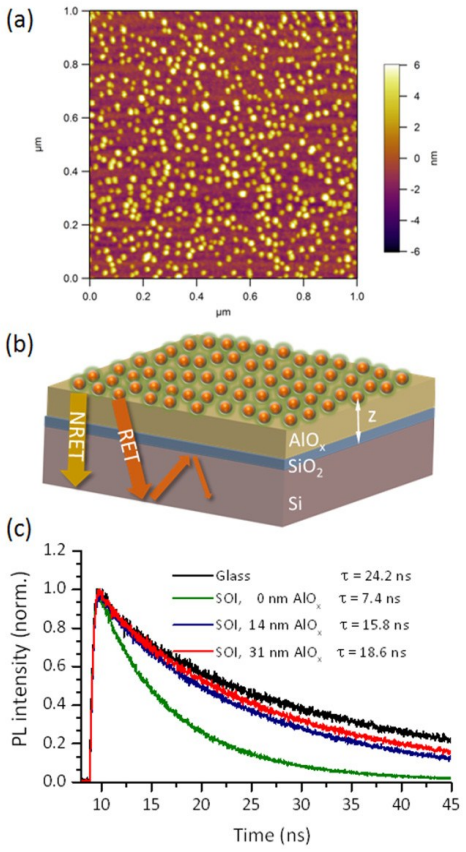

Fig. 3 (a) Atomic force microscopy micrograph of sub-monolayer CdSe/ZnS NCs deposited on top of a SOI substrate. (b) Schematic of an optical study sample consisting of sub-monolayer NCs on a SOI substrate with an AlO_x spacer. (c) Time-resolved PL decay spectra of the sub-monolayer of CdSe/ZnS NCs for different AlO_x spacer thicknesses. The PL spectrum of NCs on a glass substrate is included as a reference.

in the wavelength region below 600 nm, where the NC exhibits high optical absorption (Fig. S4†). Meanwhile, there is an excellent spectral overlap between the absorptance of ultrathin Si and the PL emission of NCs (Figs. S3(b) and S4†). These observations are consistent with the measured increase in J_{SC} of the solar cell with NC layer, while also suggesting the transfer of photon energy absorbed by the NC layer into the ultrathin Si. We plot the gain in EQE (ΔEQE), defined as EQE (with NC) – EQE (without NC), along with the simulated absorptance spectrum of the CdSe/ZnS NC layer (A_{NC}) within the device (Fig. 2(d)). A_{NC} features a spectral shape and, particularly the position of peaks, which generally match the measured ΔEQE spectrum. This strongly suggests that the energy absorbed by the CdSe/ZnS NC layer is transferred to the ultrathin Si, enhancing its light absorption and photocurrent generation.

Optical Evaluation of ET Efficiency from the NC Layer to Ultrathin Si

We obtain a more direct verification that the observed PCE enhancement is originating from ET effects by systematically studying the functional dependence of ET efficiency on the NC-Si donor-acceptor separation. Generally, the dependence of ET efficiency on the donor-acceptor separation is examined by the time-resolved PL decay measurement, a common method for investigating the extent of ET by monitoring the quenching in PL lifetime of the energy donor.[24] We employ the same method by using a CdSe/ZnS NC sub-monolayer condition that minimizes possible cross-talking among NCs and create, by and large, an idealized point-like (0D, NC) to three-dimensional (3D, ultrathin Si) energy donor-acceptor geometry, permitting an analytic dipole theory calculation. The sub-monolayer NCs were spin-coated (3000 rpm, 125 nM concentration) on SOI substrates (Si device layer thickness: 500 nm) having an AlO_x spacer coating of various thicknesses (Figs. 3(a) and (b)). The decay of NC PL for a varying AlO_x spacer thickness, d_{AlOx}, is shown in Fig. 3(c), with the PL decay of NCs on a glass substrate serving as a reference (i.e., no ET). We find that excitons in CdSe/ZnS NCs decay faster on SOI substrates as d_{AlOx} is reduced from 14 nm to 0 nm, with corresponding lifetime, τ, decreasing from 15.8 ns to 7.4 ns, which supports an efficient ET from the NCs to the ultrathin Si. We can safely exclude any potential influence of direct charge transfer from NCs to Si, considering the 1.7 nm thick silicon oxide (SiO_2) on the SOI (measured by ellipsometry) and ~3.5 nm thick polymer ligand coating on individual NCs (thus over 5 nm donor-acceptor spacing).

Meanwhile, by taking account of ~8 nm diameter of NCs (with 4.5 nm inner particle diameter), the actual separation between donor and acceptor (i.e., from the center of a NC to the surface of the ultrathin Si), z, is ranging from 19.7 down to 5.7 nm, and the observed reduction of τ by ~50% for the ~70% decrease in z is seemingly consistent with an efficient NRET induced by a stronger dipole-dipole coupling at a shorter donor-acceptor separation.[19] However, we recognize that for the 0D-3D energy donor-acceptor geometry in our samples, the rate of dipole-dipole interaction should be, in principle, proportional to $1/z^3$, predicting a more rapid change in the rate of NRET with z (e.g., τ decrease by ~97% for the z decrease from 19.7 nm to 5.7 nm) than seen in Fig. 3(c). This suggests that another mode of ET, namely RET, is most likely in operation as well. In order to specifically probe the effect of donor-acceptor separation on RET, we suppress the exciton decay via NRET by further increasing z to 36.7 nm (d_{AlOx} = 31 nm). At this distance, the PL decay is slower than those at shorter z (τ = 18.6 ns) but still faster than that on a glass substrate (i.e., no ET, τ = 24.2 ns). A modest change in the PL lifetime (from 15.8 ns to 18.6 ns) for a given increase in z (from 19.7 to 36.7 nm) is also dissimilar from the strongly z-dependent characteristics of NRET. Overall, these observations qualitatively indicate that the RET becomes a more dominant mode for ET at a long donor-acceptor separation distance. We note that the faster PL decay at d_{AlOx} = 31 nm compared with that on a glass substrate could be caused by non-zero contribution of NRET or the difference in refractive indices between AlO_x and glass (i.e., SiO_2, ~1.46)[25].

We gain further insights on the different modes of ET from the NCs to the ultrathin Si by analytically evaluating the dependence of ET rate on the donor-acceptor separation based on a physical model proposed by Malko's group.[4,15,26] By applying the Sommerfeld's treatment[27] that addresses the modification of electromagnetic fields of a classical oscillating electric dipole above a dielectric semi-space, an exciton in a NC is treated as an oscillating dipole, and the

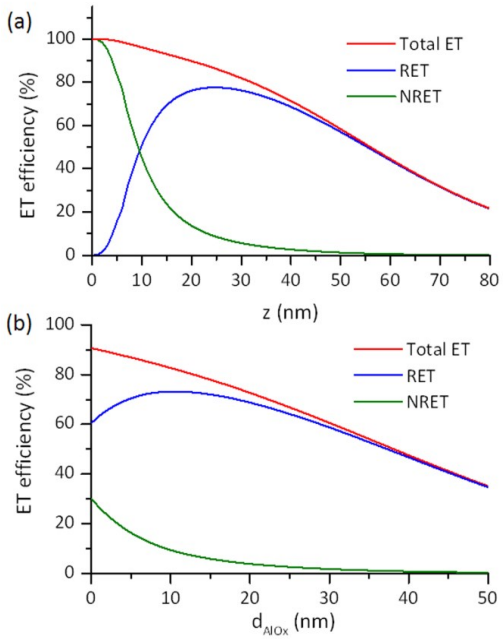

Fig. 4 Theoretically calculated efficiencies of RET (blue), NRET (green), and overall ET (red) from (a) a monolayer of CdSe/ZnS NCs and (b) four monolayers of CdSe/ZnS NCs to a 500 nm thick ultrathin Si as a function of donor-acceptor separation distance z and AlO_x spacer thickness d_{AlOx}, respectively.

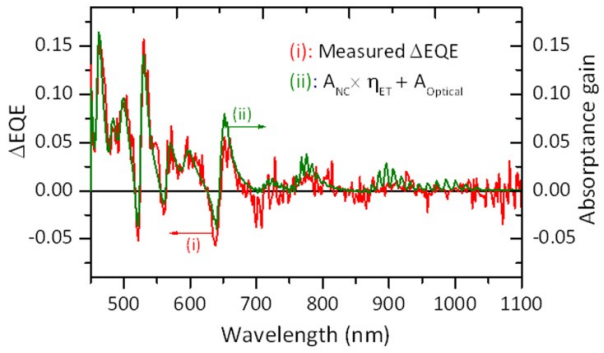

Fig. 5 Comparison of the gain in EQE (ΔEQE = EQE (with NC) – EQE (without NC), red) and the calculated total gain of light harvesting in the ultrathin Si by the addition of the NC layer, combining the contributions of ET and the anti-reflective optical effects ($A_{NC} \times \eta_{ET} + A_{Optical}$, green).

rate of exciton decay, as well as the corresponding ET efficiency, are calculated for different decay channels, including NRET, RET, and emission to vacuum (i.e., loss) in weak dipole coupling conditions, all as a function of the donor-acceptor separation distance z.

The calculated ET efficiency from a *monolayer* of NCs is plotted with respect to z (Fig. 4(a)) and confirms the efficient RET at a large donor-acceptor spacing as qualitatively predicted in our time-resolved PL measurements. The overall ET from a NC monolayer to an ultrathin Si remains very efficient with corresponding efficiency >70% even as z is approaching 40 nm, primarily owing to the effective RET whose efficiency is still >50% at z = 50 nm. On the other hand, the ET at a short donor-acceptor separation (z < 10 nm) is dominated by NRET, whose efficiency decreases exponentially with z, making its contribution to the overall ET negligible for z > 30 nm.

In order to address our actual experimental condition, we extend the ET efficiency calculation to the case of *multi-layered* NCs on an ultrathin Si, specifically four monolayers of NCs, which best represent the actual energy donor-acceptor configuration in our NC-sensitized ultrathin Si PV devices. The calculation is performed by treating each NC monolayer within the multiple NC monolayers as an independent energy donor and the NC layer(s) underneath a specific NC donor monolayer as a part of AlO_x spacer because the refractive indices of NC and AlO_x measured by spectroscopic ellipsometry are nearly identical (~1.5). We find that the calculated efficiency of inter-NC ET is less than 3.5 % (see ESI†), which supports the validity of this approach. Since the ET efficiency of each NC layers have the same functional dependence on z as the NC monolayer, normalized integration of the ET efficiencies of individual NC layers along z, assuming a uniform light absorption by each NC monolayer, yields the overall ET efficiency from the multiple monolayers of NCs to the ultrathin Si. The calculated ET efficiency from four monolayers of CdSe/ZnS NCs to a 500 nm thick Si, plotted as a function of AlO_x spacer thickness d_{AlOx} (Fig. 4(b)), reveals that the efficiency of RET is already 60% at d_{AlOx} = 0, increases to its maximum of 73% at d_{AlOx} = 10 nm, and slowly decreases thereafter. In contrast, the contribution of NRET from the four NC monolayers to the overall ET is minor as the NRET efficiency quickly drops below 10% for d_{AlOx} > 10 nm. This is caused by the fact that the actual distance z between Si surface and the center of the 2nd and above NC monolayers is already >14 nm, for which the NRET efficiency from a NC monolayer is less than 25% (Fig. 4(a)). Overall, the predicted high RET efficiency should enable an efficient overall ET from the multiple NC monolayers to the ultrathin Si for the distance of up to 50 nm, implicating a key role of RET in a practical ET-based solar cell with thick NC energy donor layers for better light absorption.

ET from NC to Ultrathin Si

Equipped with the above theoretical analyses and optical simulation data, we now find a direct proof and understanding for the relative significance of ET in the overall solar cell performance by *quantifying* the contribution of the ET mechanism to the improvement of light absorption in the ultrathin Si and resulting EQE. First, because of high PL quantum yield of our NCs (>90%), the amount of optical absorption in the NC layer that can be transferred to the ultrathin Si layer via the ET, A_{ET}, is simply: $A_{ET} = A_{NC} \times \eta_{ET}$, with η_{ET} denoting the ET efficiency from four monolayers of CdSe/ZnS NCs to 500 nm thick Si, which is 90.1% as determined from the dielectric theory calculation (Fig. 4(b), d_{AlOx} = 0). On the other hand, the NC layer allows an additional increase in the optical absorption in the ultrathin Si layer via the pure anti-reflective optical effects, $A_{Optical}$, which amounts to: $A_{Optical} = A_{Si}$ (with NC) – A_{Si} (without NC), a quantity that we can evaluate from the absorptance data obtained by the transfer-matrix optical simulation (Fig. S2 and S3†). Then, the total additional light

harvesting gain endowed by the NC layer to the ultrathin Si, ΔA_{Total}, is equal to the combined contributions from the ET and the anti-reflective optical effects: $\Delta A_{Total} = A_{ET} + A_{Optical} = A_{NC} \times \eta_{ET} + A_{Optical.}$ When we plot the calculated ΔA_{Total} spectrum along with the measured ΔEQE spectrum (Fig. 5), strikingly there is a near perfect agreement between the two spectra—this unambiguously confirms the validity of our analysis and, more importantly, proves the notion that the photon energy absorbed by the semiconductor NC layer can be efficiently converted into the enhancement in photocurrent output in the inorganic solar cell via ET.

Based on the identified individual contributions of the ET and the anti-reflective coating effects to the optical absorption of the ultrathin Si, the enhanced photocurrent output of the ultrathin Si solar cells can be analyzed in more detail, highlighting benefits of using semiconductor NCs for the excitonic ET sensitization of the active Si layer. We compare the gain in photocurrents J_{ET} and $J_{Optical}$, which are respectively originating from the ET (A_{ET}) and the anti-reflective effects ($A_{Optical}$), by calculating: $J = \int A \cdot IQE \cdot E_{AM1.5G} \cdot (e\lambda/(hc))d\lambda$, where J is the photocurrent, A is the absorptance (either A_{ET} or $A_{Optical}$), IQE is the internal quantum efficiency, $E_{AM1.5G}$ is the irradiance of AM1.5G solar spectrum (cutoff wavelength 650 nm for calculating J_{ET}, Fig. S3†), e is an elementary charge, h is the Planck constant, c is the speed of light, and λ is the wavelength. By assuming 100% IQE (IQE = 1) given the ultrathin single-crystalline Si active layer that is expected to transport free charge carriers with minimal recombination loss, we find that the photocurrent enhancement induced by the ET and the optical anti-reflective coating effects are respectively: J_{ET} = 0.55 mA/cm^2 and $J_{Optical}$ = 0.9 mA/cm^2, thus revealing ~38% of the total photocurrent enhancement induced by the NC layer (J_{Total} = 1.45 mA/cm^2) is originating directly from the ET. It is interesting to note that this much contribution of ET to the enhancement of the photocurrent output in our ultrathin Si solar cells is on par with or higher than what was reported previously in other nanostructured solar cells attempting a utilization of ET.[13,28] For instance, the polymer BHJ solar cell employing poly(3-hexylthiophene) (P3HT)/squaraine as the energy donor/acceptor couple showed that 35% of the total gain in the J_{SC} by the addition of squaraine was stemming from the ET (0.68 mA/cm^2 out of 1.94 mA/cm^2), with the rest caused by the direct charge transfer.[13] Also reported previously is the enhanced J_{SC} of nanopillar Si solar cells by 5.2% (from 6.56 to 6.90 mA/cm^2) upon the topical integration of CdSe NCs, which was much smaller than the gain in J_{SC} caused by the anti-reflective coating effects (9–14 %).[28]

Influence of Long-Range RET on the Solar Cell PV Performance

We further explore the effects of ET on the PV performance of ultrathin Si solar cells at a longer energy donor-acceptor separation (Fig. 6), where RET is expected to be dominant. The transfer-matrix optical simulation is used again to evaluate absorptances for the NC and ultrathin Si layers (A_{NC} and A_{Si}) while varying the AlO_x spacer thickness d_{AlOx} from 14, 31, 36, and to 46 nm, with or without a 35 nm thick (four monolayers) CdSe/ZnS NC layer on top (Fig. S2 and S3†).

In order to estimate the contribution from the anti-reflective optical effects by the added AlO_x spacer, we use the simulated A_{Si} to calculate the photocurrent that is generated by only a normal optical absorption (i.e., not affected by the ET) of the ultrathin Si (J_{Si}) as a function of d_{AlOx} by using the same procedure of AM1.5G integration performed earlier (Fig. 6(a)). We find that even without the NC layer, the AlO_x layer acts as an antireflective coating, increasing the coupling of the incident light into the ultrathin Si layer and therefore J_{Si}. For the surveyed range of d_{AlOx} (from 0 to 46 nm), a thicker AlO_x layer leads to a more effective anti-reflective function, increasing J_{Si} from 6.0 to 7.8 mA/cm^2. Meanwhile, with the NC layer on top, the J_{Si} increases from 6.9 to 7.9 mA/cm^2 as d_{AlOx} increases from 0 to 31 nm, but slightly decreases to 7.7 mA/cm^2 as d_{AlOx} further increases up to 46 nm. Since the application of the CdS/ZnS NC layer on top of the AlO_x layer can alter the overall optical interference in the device, the added NC layer can either increase or decrease the coupling of the incident light with the underlying ultrathin Si layer depending on d_{AlOx}.

The enhancement of J_{Si} arising from the anti-reflective optical effects after the deposition of the NC layer ($J_{Optical} = \Delta J_{Si} = J_{Si}$ (with NC) – J_{Si} (without NC), Fig. 6(b)) indeed reveals such a varying extent of optical coupling: $J_{Optical}$ increases with increasing d_{AlOx}, reaching its maximum of 1.3 mA/cm^2 at d_{AlOx} = 14 nm, but then starts decreasing thereafter for d_{AlOx} > 14 nm, causing even a negative impact on the light absorption of the ultrathin Si at d_{AlOx} = 46 nm ($J_{Optical}$ = –0.1 mA/cm^2). Unlike the decreasing photocurrent enhancement by the optical anti-reflective effects with increasing d_{AlOx}, the enhancement in photocurrent by the ET from the NC layer ($J_{ET} = J_{NC} \times \eta_{ET}$) remains significant at >0.50 mA/cm^2 for the studied range of d_{AlOx} (Fig. 6(b)) despite the decreasing η_{ET} (from 90 to 40%) for the increasing donor-acceptor separation. This occurs since the light absorption by the NC layer (A_{NC}) and the associated total available photocurrent (J_{NC}) increases significantly for a larger d_{AlOx} (e.g., J_{NC} from 0.55 to 1.40 mA/cm^2 for d_{AlOx} from 0 to 46 nm, Fig. 6(b)) due to the *improved coupling of incident light with the NC layer*. Combining the anti-reflective optical effects and the ET from the NC layer, the optimal d_{AlOx} for the highest enhancement in J_{SC} is then 14 nm in our device geometry, predicting the highest J_{Total} (= $J_{Optical} + J_{ET}$) = 2.0 mA/cm^2, all despite η_{ET} of ~79% for such a large d_{AlOx} (Fig. 6(d)). This emphasizes the importance of combining a proper light management scheme with the application of NC energy donor layer to maximize the impact of the ET-induced enhancement of the device J_{SC}. For instance, one can envision a coating of certain wave-guiding layers on top of the semiconductor NC energy donor layer in order to concentrate incident photons into the underlying NCs while protecting them from the outside environment.

The device PV performance, specifically J_{SC}, experimentally measured as a function of d_{AlOx} shows good agreements with the calculated photocurrent enhancement discussed above, confirming the effects of enhanced optical coupling by the AlO_x spacer and, more importantly, that the RET is the responsible mode for the effective ET from a thick NC layer at a long donor-acceptor separation of up to a few tens of nanometers. The average J_{SC} (measured from over 12 unique devices for each condition, Fig. S5-S8†) is plotted with respect to d_{AlOx} in Fig. 6(c) for both cases of with and without the 35 nm thick CdSe/ZnS NC energy donor layer (see Fig. S5-S8† for the summary of V_{OC}, FF, and PCE). As expected, the solar cells with the NC layer exhibit a superior J_{SC} over the control devices within the most of d_{AlOx} range, except for d_{AlOx} =

46 nm, where the control devices outputs a somewhat higher average J_{SC} than the NC-sensitized ones. Significantly, the measured enhancement in J_{SC} upon the deposition of the NC layer, $\Delta J_{SC} = J_{SC}$ (with NC) – J_{SC} (without NC), well matches the calculated photocurrent enhancement ($J_{Optical} + J_{NC} \times \eta_{ET}$) (Fig. 6(d)). The enhancement in J_{SC} remains substantial for d_{AlOx} up to 31 nm and starts decreasing for d_{AlOx} > 36 nm, further supporting the case that the ET from a thick semiconductor NC energy donor layer can remain effective even for a few tens of nanometers of energy-donor acceptor separation, afforded by the long-range RET. We note that this enhanced PV performance driven by RET is conceptually similar to what can be gained by luminescent down-shifting layers as recently studied for thin film CdTe solar cells, where the optical coupling effects were not considered.[29]

Our results support the theoretical and spectroscopic prediction [4,15,26] that RET is a long-ranged process as compared to NRET (a few tens of nanometers vs. a few nanometers), thus allowing utilization of thicker ET donor layers for efficient light harvesting in PV devices. Previous attempts to employ NRET mechanism to improve light harvesting efficiency in organic solar cells were restricted to the relatively short active-range of NRET (~a few nanometers), which limits the layer thickness or the loading amount of the additional energy donor (e.g. the optimum loading of squaraine to P3HT is only 1% in the previously mentioned example[13]). We emphasize that the efficient RET between NCs and Si layer in our system is also attributed to the specific dielectric-layered configuration (i.e., the highest refractive index of Si situated at the bottom with other components of lower refractive indices on top) in which the RET of excitons generated in the NC layer preferentially decay into wave-guiding photonic modes that propagate laterally and be absorbed within the Si layer (i.e., increasing the light path length beyond the Si thickness). The coupling of the wave-guiding modes into Si layer and RET remain efficient at a thickness of the Si layer as low as ~90 nm in our configuration (for donor emission wavelength at 605 nm and Si refractive index ~3.4), with the coupling efficiency maxima at halves of the wavelengths in Si.[4] This may be utilized to further improve the PV performances in ultrathin Si solar cells, and one of the challenges is the need for a more efficient NC light harvesting layer that can maintain high ET efficiency. As in our demonstration, where a variation in AlO_x spacer thickness significantly increased the photocurrent output by the NC layer, an incorporation of optimized dielectric component layers or coatings is expected to further improve the light harvesting by the NC layer. Another interesting direction is the utilization of a band gap-graded NC layer that exploits a cascaded ET from NCs of larger band gap to NCs of smaller band gap, and finally to underlying Si.[5,18,30] Application of plasmon-exciton coupling effects between metallic nanoparticles and NCs[31] should also provide further improvements in the PV performance of ET-based ultrathin Si solar cells.

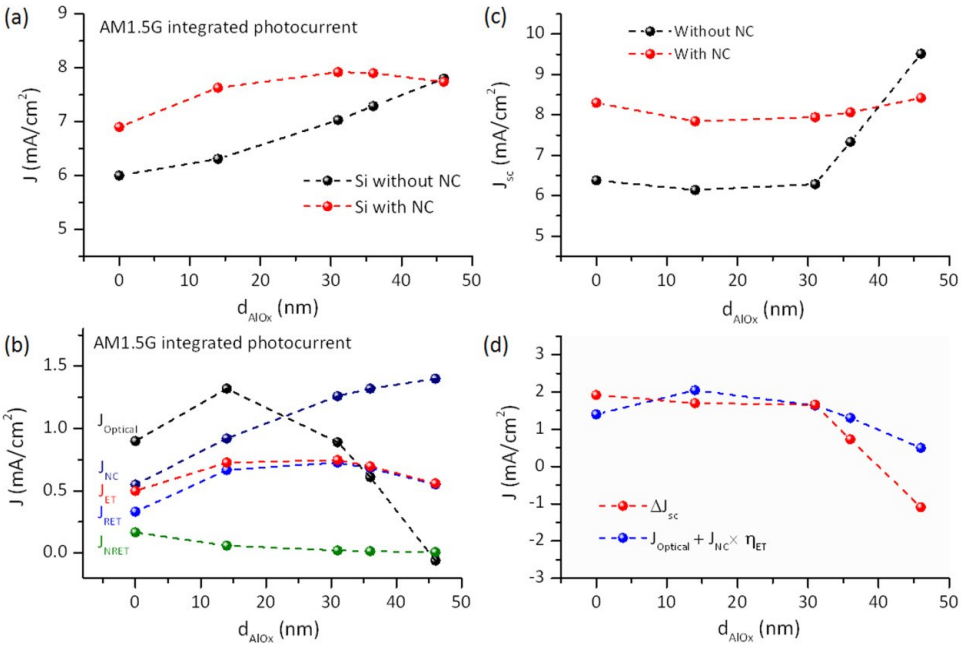

Fig. 6 (a) Simulated photocurrent outputs (J_{Si}) of ultrathin Si Schottky junction solar cells, originating from the normal optical absorptance of 500 nm thick Si layer with (red) or without (black) a 35 nm thick CdSe/ZnS NC layer, as a function of AlO_x spacer thickness d_{AlOx}. (b) Simulated enhancements in photocurrent output from the ultrathin Si caused by the anti-reflective optical effects of the NC layer ($J_{Optical}$, black) and the ET, RET, and NRET from the NC layer ($J_{ET} = J_{NC} \times \eta_{ET}$ (red), $J_{RET} = J_{NC} \times \eta_{RET}$ (blue), $J_{NRET} = J_{NC} \times \eta_{NRET}$ (green)), as a function of d_{AlOx}, with J_{NC} (navy) denoting the simulated photocurrent output from the absorptance of the NC layer. (c) Measured average J_{SC} of ultrathin Si Schottky junction solar cells vs. d_{AlOx} with (red) and without (black) a 35 nm thick CdSe/ZnS NC layer. (d) Comparison of the experimentally determined enhancement in J_{SC} (ΔJ_{SC}, red) and the calculated enhancement in photocurrent output ($J_{Total} = J_{Optical} + J_{ET}$, blue) by the NC layer as a function of d_{AlOx}. All calculated data are obtained under the 1 Sun AM1.5G condition.

3. Conclusions

In summary, we have experimentally demonstrated the positive impacts of the ET on enhancing the PV energy conversion efficiency of functioning ultrathin inorganic solar cells. The model device platform developed based on an ultrathin Si layer with an incorporated in-plane Schottky junction and the CdSe/ZnS NC energy donor layer provided precisely-defined controllable energy donor-acceptor geometry, enabling a self-consistent quantitative evaluation of the effects of ET on the device PV performances, differentiated from the classical optical coupling effects. By combining device PV characterization, dielectric theory calculations/spectroscopic measurement of the ET rate, and transfer-matrix optical simulations, we identified that the ET mechanism could provide an efficient route for light harvesting in ultrathin Si solar cells. Specifically, the 35 nm thick NC energy donor layer could enhance the J_{SC} of the 500 nm thick ultrathin Si solar cell up to ~8.7 mA/cm^2 on average by ~35%, of which ~38% is directly driven by the ET, particularly via the long-range RET. The results not only support the potential of the ET on improving the PCE of ultrathin inorganic solar cells but also provide a versatile investigative framework that can untangle and individually quantify the intricately related intrinsic optical effects and the influences of ET in developing more efficient ET-based optoelectronic devices.

4. Methods

Fabrication of Ultrathin Si Schottky Junction Solar Cells

A cleaned SOI wafer (500 nm thick device layer with resistivity of 8–11 ohm cm, 1 μm thick buried oxide, and 0.5 mm handling layer) was immersed in a buffered oxide etch solution to remove the native SiO_2 layer, followed by an annealing step at 500 °C for 10 minutes in O_2 flow to create a SiO_2 layer of ~1.7 nm. High purity Al with a thickness of ~1000 Å was thermally evaporated through a window of 750 μm × 750 μm defined by photolithography. The ohmic contact was formed by annealing the Al contact at 600 °C for 45 seconds under Ar using a rapid thermal processor. The Schottky contact was formed by depositing 1000 Å thick Al through another window of 750 μm × 750 μm, aligned in parallel with the ohmic contact with a 10 μm channel. The surrounding Si layer was etched away via reactive ion etching using a gas mixture of CHF_3 and SF_6 in order to define an active device area of 10 μm × 750 μm. The fabricated devices were then annealed under Ar at 450°C for 5 minutes, followed by a 150 °C sintering in a vacuum oven for 36 hours to stabilize the PV performance characteristics.

Semiconductor NC Deposition

The water-soluble CdSe/ZnS NCs with the emission wavelength of λ_o = 605 nm were purchased from Invitrogen and used as received. It is noted that these NCs are air-stable and suitable for ambient device and optical characterization. The long polymer ligand coating on NCs is beneficial for suppressing any direct charge transfer and inter-NC NRET. One may utilize an optimized, shorter polymer coating to enhance ET and PV performance while preventing the charge transfer. The NC solution (8 μM concentration) was spin-coated on the open channel of the fabricated ultrathin Si solar cell at 3000 rpm. The sample was then dried by keeping it in a fume hood for ~ 30 min. The PV characterization of devices with NC was usually conducted within a day after NCs was deposited. Several samples were tested over 3 days, and they showed no significant degradation in PV characterization, indicating a good ambient stability of NCs. The thickness of the NC layers was 30–35 nm as determined by SEM and ellipsometry measurements. In addition, a NC solution diluted 64× by a phosphate buffer solution (pH = 7) was spin-coated on SOI and Si substrates with the contact structure to obtain a sub-monolayer coverage of NCs for the time-resolved PL measurement. The PL quantum yield for NCs in colloidal solution was provided by the manufacture (Invitrogen).

AlO_x Spacer Deposition and Characterization

The AlO_x spacer layer with controlled thicknesses were deposited on devices, SOI, Si, and glass substrates via ALD at 85 °C using tetramethylammonium and water as precursors. The thickness and refractive index of the deposited AlO_x layers were measured by variable-angle spectroscopic ellipsometry. The measured refractive index of ALD-deposited AlO_x (~1.5 at 605 nm) was smaller compared with that of sapphire (~1.8), most likely due to its lower density as confirmed by X-ray reflectivity measurement (data not shown). We also tested possible photoionization or photocharging of the ALD-AlO_x layer from NCs by measuring the PL decay of sub-monolayer NCs on glass substrates with or without 5 nm ALD-AlO_x.layer. No significant difference was observed between two types of substrates, confirming the absence of charge transfer from the NCs to ALD-deposited AlO_x.

PV Characterization

All PV characterization of devices was performed in ambient air at room temperature. Dark and illuminated *J-V* characteristics of solar cells were measured under the 1 Sun AM1.5G condition by using a custom-modified electrical probe station equipped with a precision semiconductor parameter analyzer (Agilent) and a 150 W solar simulator (Newport). The 1 Sun AM1.5G illumination condition was verified by a calibrated quartz-windowed Si reference solar cell (Newport, NIST-traceable) and cross-checked by a spectrometer calibrated for an absolute spectral irradiance measurement. The EQE of solar cells was measured by using a calibrated UV-enhanced Si photodiode (Newport) and a wavelength-variable monochromatic light source (a 300 W xenon arc lamp combined with a monochromator, Newport) along with the electrical probe station.

Variable-Angle Spectroscopic Ellipsometry

All measurements were made using a J.A. Woollam V.A.S.E. M-2000 ellipsometer in an ambient air at room temperature. Active material (CdSe/ZnS NCs) was spin-coated on three different substrates, including a microscope slide glass, a SOI substrate, and a Si substrate. It was assumed that the optical properties of the active layers on all three substrates were identical, such that any changes in the acquired spectra could be attributed to the variation in substrate characteristics. This procedure produces multiple sets of unique data for a given condition, allowing a greater statistical confidence of data fitting to a parametrized model. Ellipsometric measurements were first conducted on the cleaned bare substrates for the

wavelength range of 210–1700 nm at the incidence angle from 45 to 80 degrees (5 degree interval). The large range of incidence angle not only includes the Brewster angle for each of the substrates at which the sensitivity of the measurement is highest but also increases the dataset thereby reducing the parameter correlations in the fitting process and the sensitivity to any composition variation over the film. The data collected from the three substrates were then analyzed simultaneously by using the WVASE32 software (version 3.770, J.A. Woollam Co.) to yield solutions for the complex refractive index and the film thickness by performing data fitting using the Levenberg-Marquardt multivariate regressions algorithm. The collected data consists of the complex ratio of the reflection amplitudes of polarized light with electric field within (r_p) and perpendicular (r_s) to the plane of incidence as a function of the angle of incidence. From this data, plots of ψ and Δ versus angle of incidence were determined from the definition of ψ and Δ: $r_p/r_s = \tan(\psi)\cdot e^{i\Delta}$.

Time-Resolved PL Lifetime Measurements

We used a custom-built confocal scanning stage microscope based on an inverted microscope, equipped with a piezo scanning stage (Physik Instruments, Germany) and a 405 nm pulsed (10 MHz) diode-pumped solid-state laser light source. The average input light power at the sample was kept at ~2 μW. The PL signal was collected in the epi-illumination scheme, where the signal is spectrally separated from the excitation laser light by a dichroic (Semrock, DiO-532) and a band-pass filter (Semrock FF01-605/50 for NC605). The resulting signal was spatially filtered by a 75 μm pinhole and finally imaged onto a single photon counting avalanche photodiode (MPD Picoquant) coupled to a time-analyzer (PicoHarp 300, PicoQuant). Data acquisition and analysis were performed by the Symphotime analysis software (Picoquant). The time-resolved PL decay data, fitted with a multi-exponential function, provide amplitude-averaged exciton lifetimes in NCs since there is only one type of fluorophore (NCs) in our system.[19,32]

Acknowledgements

This research was carried out at the Center for Functional Nanomaterials (S.H., D.N, C.-Y.N.) and Sustainable Energy Technologies Department (A.A. and M.D.E.), Brookhaven National Laboratory (BNL), which is supported by the U.S. Department of Energy, Office of Basic Energy Sciences, under Contract No. DE-SC0012704.

References

1 G. D. Scholes, Long-range Resonance Energy Transfer in Molecular Systems, *Annu. Rev. Phys. Chem.,* 2003**,** 54, 57-87.

2 G. S. Engel; T. R. Calhoun; E. L. Read; T.-K. Ahn; T. Mancal; Y.-C. Cheng; R. E. Blankenship; G. R. Fleming, Evidence for Wavelike Energy Transfer through Quantum Coherence in Photosynthetic Systems, *Nature,* 2007**,** 446, 782-786.

3 Y. C. Cheng; G. R. Fleming, Dynamics of Light Harvesting in Photosynthesis, *Ann. Rev. Phys. Chem.,* 2009**,** 60, 241-262.

4 H. M. Nguyen; O. Seitz; W. Peng; Y. N. Gartstein; Y. J. Chabal; A. V. Malko, Efficient Radiative and Nonradiative Energy Transfer from Proximal CdSe/ZnS Nanocrystals into Silicon Nanomembranes, *ACS Nano,* 2012**,** 6, 5574-5582.

5 A. Yeltik; B. Guzelturk; P. Ludwig Hernandez-Martinez; S. Akhavan; H. Volkan Demir, Excitonic Enhancement of Nonradiative Energy Transfer to Bulk Silicon with the Hybridization of Cascaded Quantum Dots, *Appl. Phys. Lett.,* 2013**,** 103, 261103.

6 J. I. Basham; G. K. Mor; C. A. Grimes, Förster Resonance Energy Transfer in Dye-Sensitized Solar Cells, *ACS Nano,* 2010**,** 4, 1253-1258.

7 B. E. Hardin, Increased Light Harvesting in Dye-Sensitized Solar Cells with Energy Relay Dyes, *Nature Photon.,* 2009**,** 3, 406-411.

8 L. Novotny; N. Van Hulst, Antennas for light, *Nature Photon.,* 2011**,** 5, 83-90.

9 W. Zou; C. Visser; J. A. Maduro; M. S. Pshenichnikov; J. C. Hummelen, Broadband Dye-Sensitized Upconversion of Near-Infrared Light, *Nature Photon.,* 2012**,** 6, 560-563.

10 C. J. Bardeen, The Structure and Dynamics of Molecular Excitons, *Annu. Rev. Phys. Chem.,* 2014**,** 65, 127-148.

11 J. Fan; M. Hu; P. Zhan; X. Peng, Energy Transfer Cassettes Based on Organic Fluorophores: Construction and Applications in Ratiometric Sensing, *Chem. Soc. Rev.,* 2013**,** 42, 29-43.

12 K. Shankar; X. Feng; C. A. Grimes, Enhanced Harvesting of Red Photons in Nanowire Solar Cells: Evidence of Resonance Energy Transfer, *ACS Nano,* 2009**,** 3, 788-794.

13 J.-S. Huang; T. Goh; X. Li; M. Y. Sfeir; E. A. Bielinski; S. Tomasulo; M. L. Lee; N. Hazari; A. D. Taylor, Polymer Bulk Heterojunction Solar Cells Employing Forster Resonance Energy Transfer, *Nature Photon.,* 2013**,** 7, 479-485.

14 K. Cnops; B. P. Rand; D. Cheyns; B. Verreet; M. A. Empl; P. Heremans, 8.4% efficient fullerene-free organic solar cells exploiting long-range exciton energy transfer, *Nat. Commun.,* 2014**,** 5, 3406.

15 M. T. Nimmo; L. M. Caillard; W. De Benedetti; H. M. Nguyen; O. Seitz; Y. N. Gartstein; Y. J. Chabal; A. V. Malko, Visible to Near-Infrared Sensitization of Silicon Substrates via Energy Transfer from Proximal Nanocrystals: Further Insights for Hybrid Photovoltaics, *ACS Nano,* 2013**,** 7, 3236-3245.

16 S. Lu; Z. Lingley; T. Asano; D. Harris; T. Barwicz; S. Guha; A. Madhukar, Photocurrent Induced by Nonradiative Energy Transfer from Nanocrystal Quantum Dots to Adjacent Silicon Nanowire Conducting Channels: Toward a New Solar Cell Paradigm, *Nano Lett.,* 2009**,** 9, 4548-4552.

17 S. Lu; A. Madhukar, Nonradiative Resonant Excitation Transfer from Nanocrystal Quantum Dots to Adjacent Quantum Channels, *Nano Lett.,* 2007**,** 7, 3443-3451.

18 W. J. I. De Benedetti; M. T. Nimmo; S. M. Rupich; L. M. Caillard; Y. N. Gartstein; Y. J. Chabal; A. V. Malko, Efficient Directed Energy Transfer through Size-Gradient Nanocrystal Layers into Silicon Substrates, *Adv. Funct. Mater.,* 2014**,** 24, 5002-5010.

19 A. Yeltik; B. Guzelturk; P. L. Hernandez-Martinez; A. O. Govorov; H. V. Demir, Phonon-Assisted Exciton Transfer into Silicon Using Nanoemitters: The Role of Phonons and Temperature Effects in Förster Resonance Energy Transfer, *ACS Nano,* 2013**,** 7, 10492-10501.

20 W. N. Peng; S. Sampat; S. M. Rupich; B. Anand; H. M. Nguyen; D. Taylor; B. E. Beardon; Y. N. Gartstein; Y. J.

Chabal; A. V. Malko, Hybrid light sensor based on ultrathin Si nanomembranes sensitized with CdSe/ZnS colloidal nanocrystal quantum dots, *Nanoscale,* 2015**,** 7, 8524-8530.
21 M. Dutta; L. Thirugnanam; P. Van Trinh; N. Fukata, High Efficiency Hybrid Solar Cells Using Nanocrystalline Si Quantum Dots and Si Nanowires, *ACS Nano,* 2015**,** 9, 6891-6899.
22 R. Hezel; R. Schörner, Plasma Si Nitride—A Promising Dielectric to Achieve High-Quality Silicon MIS/IL Solar Cells, *J. Appl. Phys.,* 1981**,** 52, 3076-3079.
23 http://sjbyrnes.com/fresnel-solver.nb
24 F. T. Rabouw; S. A. den Hartog; T. Senden; A. Meijerink, Photonic Effects on the Förster Resonance Energy Transfer Efficiency, *Nat. Commun.,* 2014**,** 5, 3610.
25 I. H. Malitson, Interspecimen Comparison of Refractive Index of Fused Silica, *J. Opt. Soc. Am.,* 1965**,** 55, 1205-1208.
26 H. M. Nguyen; O. Seitz; D. Aureau; A. Sra; N. Nijem; Y. N. Gartstein; Y. J. Chabal; A. V. Malko, Spectroscopic Evidence for Nonradiative Energy Transfer between Colloidal Cdse/Zns Nanocrystals and Functionalized Silicon Substrates, *Appl. Phys. Lett.,* 2011**,** 98, 161904.
27 A. Sommerfeld, *Partial Differential Equations in Physics*. Academic Press: New York, 1964.
28 B. Güzeltürk; E. Mutlugün; X. Wang; K. L. Pey; H. V. Demir, Photovoltaic Nanopillar Radial Junction Diode Architecture Enhanced by Integrating Semiconductor Quantum Dot Nanocrystals as Light Harvesters, *Appl. Phys. Lett. ,* 2010**,** 97, 093111.
29 S. Kalytchuk; S. Gupta; O. Zhovtiuk; A. Vaneski; S. V. Kershaw; H. Y. Fu; Z. Y. Fan; E. C. H. Kwok; C. F. Wang; W. Y. Teoh; A. L. Rogach, Semiconductor Nanocrystals as Luminescent Down-Shifting Layers To Enhance the Efficiency of Thin-Film CdTe/CdS and Crystalline Si Solar Cells, *J Phys Chem C,* 2014**,** 118, 16393-16400.
30 T. Franzl; T. A. Klar; S. Schietinger; A. L. Rogach; J. Feldmann, Exciton Recycling in Graded Gap Nanocrystal Structures, *Nano Lett.,* 2004**,** 4, 1599-1603.
31 T. Ozel; P. L. Hernandez-Martinez; E. Mutlugun; O. Akin; S. Nizamoglu; I. O. Ozel; Q. Zhang; Q. Xiong; H. V. Demir, Observation of Selective Plasmon-Exciton Coupling in Nonradiative Energy Transfer: Donor-Selective versus Acceptor-Selective Plexcitons, *Nano Lett.,* 2013**,** 13, 3065-3072.
32 A. Sillen; Y. Engelborghs, The Correct Use of "Average" Fluorescence Parameters, *Photochem. Photobiol.,* 1998**,** 67, 475-486.